Journal of Solid State Chemistry **145,** 50–57 (1999)
Article ID jssc.1999.8215, available online at http://www.idealibrary.com on IDEAL®

Preparation of Ultrafine Nickel Ferrite Powders Using Mixed Ni and Fe Tartrates

J. M. Yang, W. J. Tsuo, and F. S. Yen

Department of Mineral and Petroleum Engineering, National Cheng Kung University, Tainan, Taiwan 70101, Republic of China

Received September 1, 1998; in revised form February 12, 1999; accepted February 13, 1999

Ultrafine nickel ferrite powders of 10 nm in particle size were prepared by the calcination of gel powders of coprecipitated Ni- and Fe-containing tartates at 250° to 400°C/2 h. The gel powder was a mixture of Ni and Fe tartrates exhibiting characteristics of the individual salts. The mixing homogeneity of the two salts strongly influenced the history of thermal reaction and the characteristics of the powder thus obtained. Both the formation temperature and the particle size increased with the retrograde of the mixing state, which initiated the increase in crystallite sizes of the intermediates, γ-Fe_2O_3 and NiO or Ni metal phases. Defect nickel ferrite spinel was formed if the oxygen fugacity was lower. Defect ferrites, especially those obtained at lower calcination temperatures, were highly susceptible to thermal decomposition at higher temperatures. © 1999 Academic Press

Key Words: **nickel ferrite; spinel; defect structure; tartrate; thermal decomposition; particle size.**

INTRODUCTION

Solid state reaction techniques (1–2) are used to prepare ferrite powders. During the preparation, the initial materials, which are mostly metal oxides, are well mixed and then calcined at high temperatures. Since the particle size of these metal oxides can vary, with a maximum size of more than several micrometers, and the mixing operation may reach different degrees of "well-mixing," the calcination temperature is relatively high. Powders obtained are generally coarse-grained and residual, with additional mineral phases sometimes also present. This results in a substantial relaxation loss and a lower capability for magnetization if ceramic magnets are fabricated using the powders.

Ultrafine (i.e., nanosize) spinel ferrite powders have been extensively studied due to their specific magnetic properties, which can be used for magnetic fluids (3) or in the fabrication of high quality electromagnetic devices. Such spinel ferrites are mostly synthesized by innovative methods, including hydrothermal systems, freeze drying, spray drying, chemical coprecipitation, and sol-gel processes (4–10). Methods for low temperature preparation of controlled grain size (11) and monophasic nickel ferrite and similar materials have been described (12). These studies mainly focused on developing techniques for preparing stoichiometric and monophase ultrafine ferrite powders. Preparation of monodispersed fine particles and composite natures in varying shapes, ranging in size from several nanometers to several micrometers, have also been reported (13–16).

The most important issue for employing innovative techniques in preparing multicomponent compounds is obviously the principle of mixing the raw materials well during the synthesis of the new compounds. A thorough mixing system can eliminate or reduce the diffusion path in the solid state reaction (17–19). A state is generally considered well mixed if the particle size of the starting materials, for example, metal oxides, is nanometer-sized or smaller and the starting materials are homogeneously mixed on an "atomic scale" (20–22). Or, in the present case, "well mixed" means that the shortest diffusion path for the atoms is during the thermal reaction. Thus, the formation of a new phase can be obtained at a lower process temperature, in comparison to conventional solid state reactions using market-purchased metal oxides as their starting materials. This is because powders with coarser particle sizes will have lower degrees of mixing from the viewpoint of a diffusion path among the reacting atoms. During thermal reactions, the well-mixed ultrafine powders will be conducted through their shorter diffusion paths and by the driving force offered by the surface tension. Contrarily, for coarser particles, as the surface tension is lowered, the diffusion path becomes longer and higher temperatures are required to provide the necessary energy for the reaction.

The present investigation deals with the synthesis of ultrafine $NiFe_2O_4$ powders using tartrate precursor techniques. The precursor obtained by chemical coprecipitation techniques is aged in solutions with varying pH environments to modify the surface properties and the mixing states of the particles. The study also presents an attempt to correlate the mixing degree of the precursors with the resulting particle size of newly formed nickel ferrite powders. Genetic sequences of the mineral phase that

0022-4596/99 $30.00

formed during the thermal treatment for the precursors are also described.

EXPERIMENTAL PROCEDURE

Precursor Preparation

Reagent-grade nickel acetate ($Ni(CH_3COOH)_2 \cdot 2H_2O$, Ferak), ferric nitrate ($Fe(NO_3)_3 \cdot 9H_2O$, Ferak), and tartaric acid ($C_4H_6O_4$, Ferak) were dissolved in ethyl alcohol (99.5%, Seoul). The concentrations of the Ni^{2+}, Fe^{3+}, and tartaric acid were then determined to be 0.065, 0.125, and 0.290 mol/L, respectively. A solution containing Ni^{2+} and Fe^{3+} in a molar ratio of Ni : Fe = 1 : 2 was prepared using the Ni^{2+} and Fe^{3+} solutions. Precipitates were then obtained by titrating the as-prepared solution into the stirred tartaric acid solution. The quantity of the tartaric acid was 20% in excess over the stoichiometric amount required to meet the charge balance. The precipitates remained in the solution (in the original container) for 0.5 h with constant stirring to ensure that the reaction was complete. Then, the resulting solution was pH-value adjusted by the addition of NH_4OH solution (0.5 N). Six samples with different pH values of 1, 3, 5, 7, 8, and 9 were prepared in this study. The samples were then aged for 1 h at room temperature with constant stirring. The precipitate was then separated from the solution using a Buchner funnel. During the separation process, a substantial difference resulting from the pH treatment was observed in that a manifested flocculation that brought about a higher speed of filtration occurred with the higher pH treated samples. The Ni/Fe mole ratio of the precipitate was then examined through chemical analysis on the residual solution using inducing coupled plasma (ICP) techniques. The analysis revealed that similar amounts of precipitates, close to 1/2, were recovered from the samples obtained at pH = 3, 5, 7, and 8. However, smaller amounts of Ni^{2+} cations were detected in the solutions at pH 1 and 9 (Table 1). The latter two were not used for further experimental work. The precipitated gel was cleaned by resuspending in pure alcohol and filtering again to remove NO_3^-, CH_3COO^-, and $C_4H_4O_4^{2-}$ ions. Washing and filtration were repeated three times before the precipitate was dried at 75°C for 24 h. The dried gel was ground to -200 mesh (<74 μm) and used as the starting material for the investigation. It was also noted that gel powders produced from high pH treatments were more like the spray-dried milk variety.

Additionally, gel powders of both pure Ni^{2+} and pure Fe^{3+} were obtained separately following identical procedures without pH adjustment.

TABLE 1
Amount of Precipitation of Ni and Fe with Various pH Values

pH	1	3	5	7	8	9
Fe (%)[a]	99.90	99.98	99.99	99.97	99.96	99.96
Ni (%)	99.82	99.95	99.98	99.95	99.86	99.45

[a] % is relative to initial concentrations of Ni and Fe.

Calcined Powders

A preliminary test using differential thermal analysis/thermogravimetric analysis (DTA/TG) was made to evaluate the necessary temperature and the process for calcination of the gel powder (starting material). Two types of thermal treatment with oxygen fugacity at temperatures 200 to 600°C at the interval of 50 or 100°C were employed for 2 h. The heating rate was 5°C/min.

Characterization

The crystalline phases in the gel and the calcined powders were identified by XRD powder methods using Ni-filtered Cu$K\alpha$ radiation (Rigaku, Tokyo). Specific surface areas were measured using the conventional nitrogen absorption (BET) technique (Gemini 2360, Micromeritics). Equivalent spherical diameters (surface diameter) were calculated from the surface areas assuming the shape factor was 6.

Thermal behavior examinations of the gel powder were conducted using DTA/TGA techniques (Setaram TGA92) in air at a heating rate of 10°C/min.

RESULTS AND DISCUSSION

Thermal Behaviors of Ni^{2+} and Fe^{3+} Gel Powders

Figures 1a and 1b display DTA/TG curves of the Ni^{2+} and the Fe^{3+} containing gel powders. The corresponding XRD diffraction patterns are shown in Fig. 2. Both gels were obtained from the solution without pH value adjustments (pH < 2).

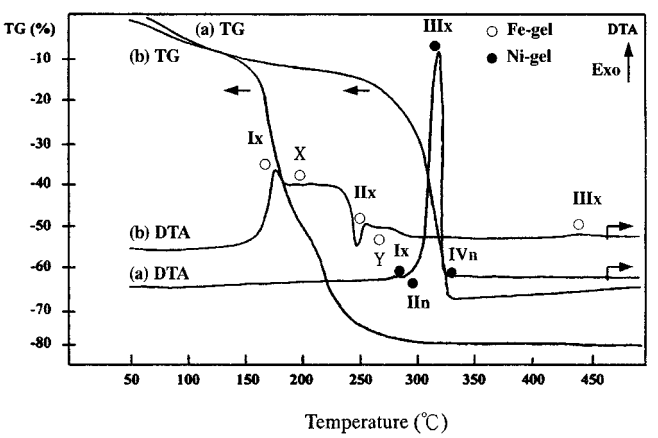

FIG. 1. DTA/TG curves of (a) pure nickel-containing gels and (b) pure iron-containing gels.

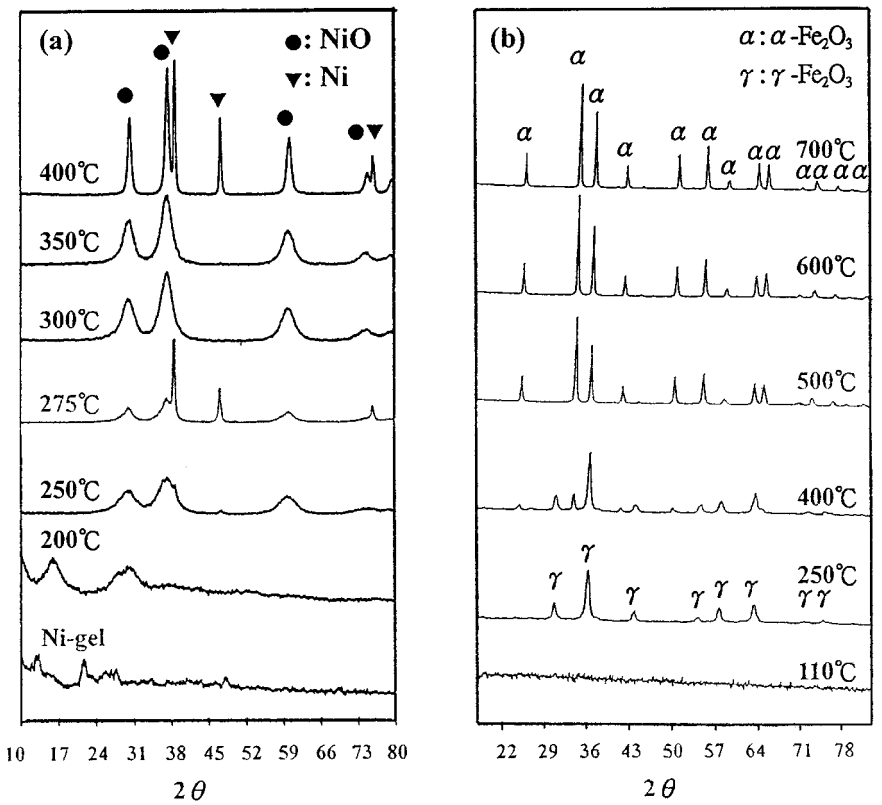

FIG. 2. X-ray diffraction patterns for nickel and iron-containing gel powders after being calcined at various temperatures. (a) Nickel gels and (b) iron gels.

Three exothermic reactions occurred at temperatures 270–320 (I*x*), 300–350 (III*x*), and >340°C (IV*x*) for the nickel-containing gel powders (Fig. 1a). Meanwhile, there were possibly two endothermic reactions which took place at 285–310 (II*n*) and 325–380°C (IV*n*) that intercepted the high temperature ends of the exothermic peaks I*x* and III*x*, respectively. To determine the thermal reactions, phase identifications using XRD techniques for the calcined powders that calcined at the corresponding temperatures were performed (Fig. 2a). The exotherm III*x* resulted from the thermal decomposition of the tartrate. During the decomposition, first NiO appeared (I*x*, 270°C), concurrently accompanied with the occurrence of a trace of Ni metal (II*n*). The latter was then oxidized to NiO following heating (V*x*, >340°C). However, on subsequent annealing at 400°C/2h, the Ni reappeared (Fig. 2a), although it cannot be observed on the DTA curves.

Judging from TG analysis, the substantial weight loss (accompanied with the exotherm III*x*) terminated abruptly at 325°C. This may indicate the beginning of a weight gain (IV*x*). Furthermore, this can be related to the disappearance of Ni or the formation of NiO ($Ni + 1/2O_2 \rightarrow NiO$) and can be evidenced by XRD phase identifications. Moreover, the following weight gain beginning at 325°C released the Ni metal that was formed at endotherm; II*n* transferred to NiO by oxidation once the temperature was over 325°C.

For ferric iron containing gel powders, a broad exothermic reaction occurred at the temperature range 150–250°C (Fig. 1b). Judging from the weight loss, this was achieved via the thermal decomposition of tartrate. The detailed process was not identified. From further examinations of XRD profiles of the calcined powders that were treated at the selected temperatures, it was noted that γ-Fe_2O_3 can be formed as the heating temperature rises above 250°C (II*x*, Fig. 1b). Compared with the TG profile, the initiation of the exothermic reaction, accompanied with a weight-gain reaction, implied that before the occurrence of II*x* an endothermic reaction took place (designated as *X*, at 175–245°C) (23). The endotherm presumably consisted of the formations of Fe^{2+} and Fe^{3+} (γ-Fe_2O_3, Fig. 2b). Finally the exothermic peak observed at temperature 440–460°C was then attributed to the phase transformation of γ- to α-Fe_2O_3 (III*x*, Fig. 2b), corresponding to the XRD profile of 400°C (annealed for 2 h). A weight loss of about 4% was measured, implying that the oxygen content of γ-Fe_2O_3 with the spinel structure was higher than that of α-Fe_2O_3 with a corundum structure. Table 2 outlines the individual thermal behaviors of Ni- and Fe-containing gel powders.

TABLE 2
Thermal Behaviors of Individual Gels Containing Ni and Fe

Ni-gels		Fe-gels	
Temp. (°C)	Process	Temp. (°C)	Process
		I*x* 150–250	Tartrates decomposition
		X 160–240?	Fe^{2+} formation (23)
		II*x* 250–275	γ-Fe_2O_3 formation
I*x* 285–325	NiO formation	*Y* 275?	
II*n* 285–310?	$NiO \rightarrow Ni + 1/2O_2$		
III*x* 300–350	Tartrates decomposition		
IV*n* 325–380	$NiO \rightarrow Ni + 1/2O_2$		
V*x* > 340	$Ni + 1/2O_2 \rightarrow NiO$		
		III*x* 440–460	$\gamma \rightarrow \alpha$-$Fe_2O_3$

Thermal Behaviors of Ni–Fe Coprecipitates

Figures 3a–c, and (d) show DTA/TG curves for the various pH aged gel powders. All samples consisted of a mixture of Ni- and Fe-containing gels. The curves exhibited individual characteristics of the Ni and Fe gel powders with substantial discrepancies. The prominent exothermic reaction, which occurred at the temperature range of 190–240°C accompanied by an enormous weight loss, was the thermal decomposition of Fe-tartrate (I*x*). The burning action seemed to trigger another thermal decomposition of the Ni-tartrate (I*x*′) (Fig. 3c, pH 7). Close to the exothermic reactions, there was an endothermic reaction (II*n*) which occurred at the temperature range 220–280°C. This brought a substantial increase in sample weight, revealing that, besides the reducing atmosphere which caused the presence of Fe^{2+}, discernable reactions for formations of NiO and γ-Fe_2O_3 also followed. The curve on the high temperature wing of peak II*n* flattened, revealing that there can be one or more than one reaction existing in this temperature region. The weight gain observed for TG evidently supports the assumption that the sample underwent an oxidizing reaction. Among these reactions, it is noted that at the temperature where γ-Fe_2O_3 appeared, III*x* ascended and the peak manifested with the increase of pH values (refer to Fig. 3d, 266°C). The α-Fe_2O_3 phase appeared at approximately 450°C (Fig. 3), regardless of the pH values employed.

Formation of Nickel Ferrite

XRD examinations on the powders of pH aged gel for various heat treatments are given in Fig. 4. It is clear that γ-Fe_2O_3 and Ni metal and NiO were formed at temperatures below 250°C. Further, since γ-Fe_2O_3 and nickel ferrite both have similar spinel structures, the formation of nickel ferrite using γ-Fe_2O_3 and Ni or NiO as the starting materials can belong to a topotectic reaction. Thus, a lower formation temperature was possible. When the XRD results were correlated with the previous DTA/TG curves, the concerned nickel–ferrite was produced at a temperature range of 280–420°C, giving rise to the exothermic reaction IV*x* (Fig. 3). The results obtained by both XRD and DTA/TG were consistent. The peak temperature, however, was at ~287°C for gels aged using pH 3 (IV*x*, Fig. 3a). With increasing pH values, the temperature increased from 287 to 417°C as the pH increased from 3 to 8. Moreover, it eventually separated further from the exotherm III*x*. Since the exothermic reaction III*x* resulted from the formation of γ-Fe_2O_3 , and since nickel ferrite was formed by diffusing Ni atoms into the spinel structure of γ-Fe_2O_3 (24), the leaving of IV*x* from III*x* to a higher temperature certainly implies that a higher reaction temperature was needed for the formation of nickel ferrite if higher pH values were employed.

The appearance of nickel ferrite was closely succeeded by a continuous weight-gain reaction to higher temperatures, indicating that a defect structure occurred in the ferrite. Regarding the XRD examinations of the samples heat treated at 600°C, it is obvious that higher pH treated ferrite

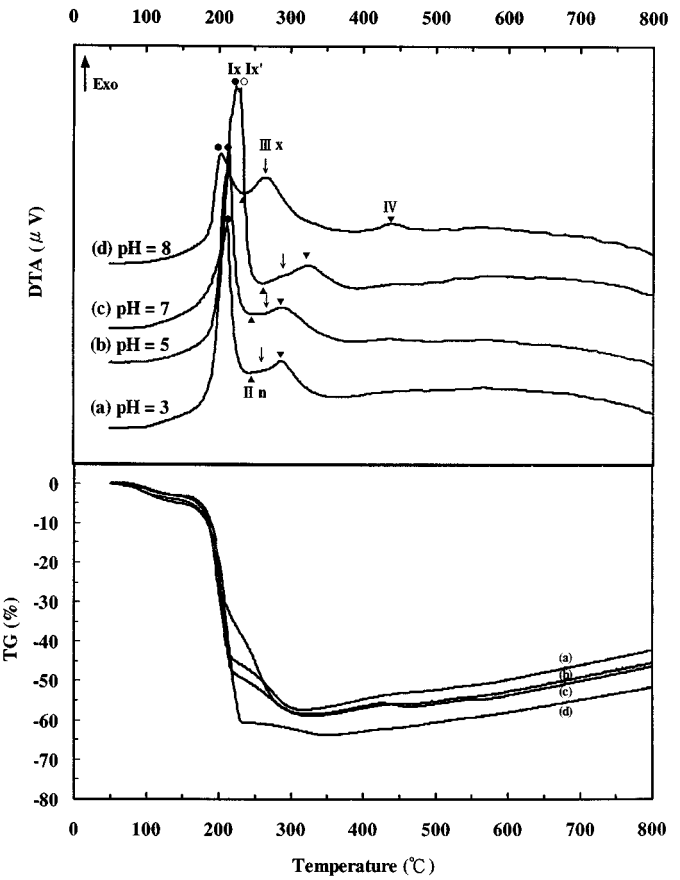

FIG. 3. DTA/TG curves for the pH aged gel (Ni–Fe coprecipitates) powders. (a) pH 3, (b) pH 5, (c) pH 7, and (d) pH 8.

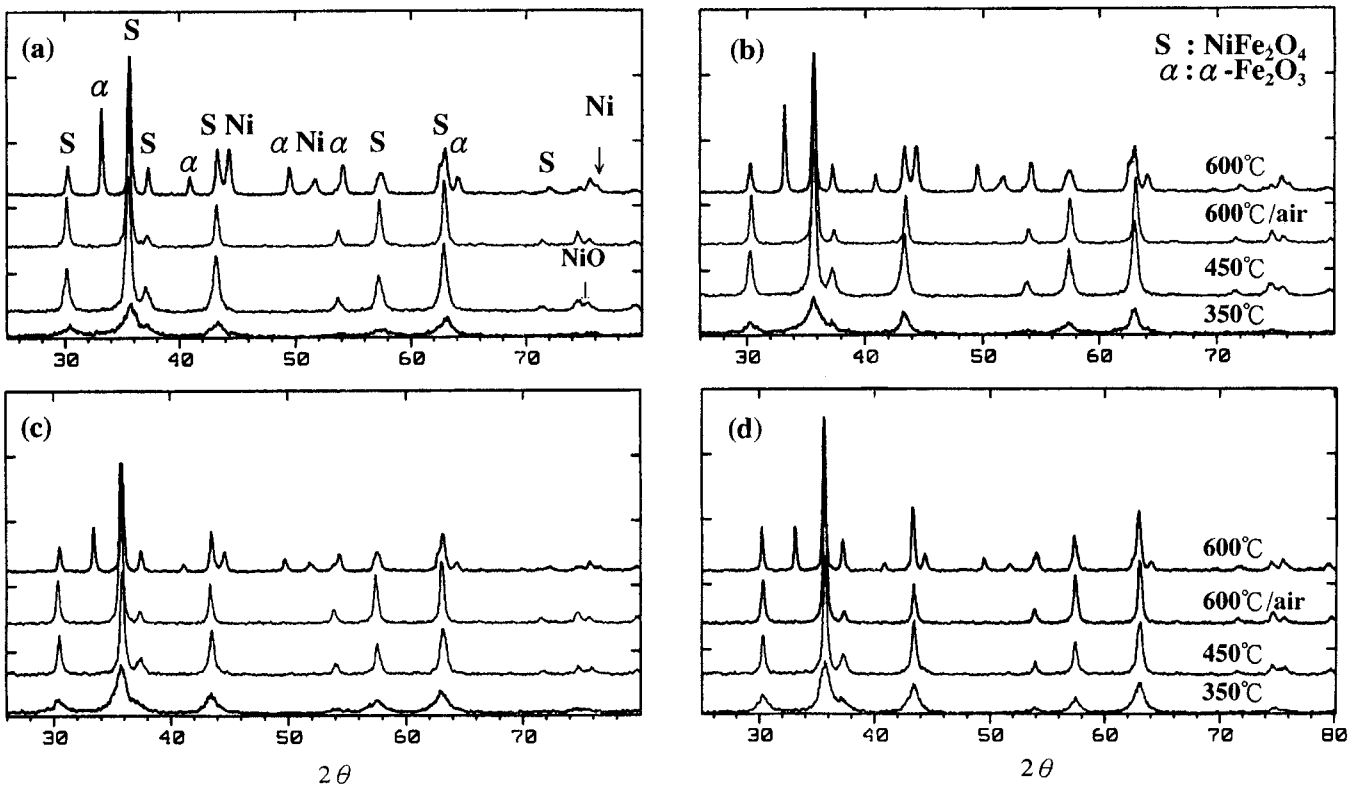

FIG. 4. X-ray examinations of the pH aged gel (Ni–Fe coprecipitates) powders calcined at various temperatures. (a) pH 3, (b) pH 5, (c) pH 7, and (d) pH 8.

owned a greater capability to sustain thermal decomposition into α-Fe_2O_3 and Ni metal (Fig. 4). As nickel ferrite was obtained using starting materials treated at higher pH solutions which required higher formation temperatures, the results imply that nickel ferrite formed at lower temperatures possesses higher defect structure that eventually reduced the high temperature stability (Fig. 5). Figure 6 demonstrates the DTA/TG curve of nickel ferrite powders obtained at 350°C/2 h with an air leak into the calcination furnace. The gel powder was treated using pH 5. It is noteworthy to find that the weight-gain behavior and the formation of α-Fe_2O_3 were eliminated.

Particle Size (by BET)

Table 3 shows the particle size (surface area diameter, measured by the BET method) variation of the nickel ferrite powder calcined at 350, 450, and 600°C for 2 h. For comparison, powders calcined at 350 and 600°C/2h on a slight exposure to air during the calcination procedure were also included. It was found that all newly formed nickel ferrite powders had mean particle sizes of about 10 nm. As usual, higher calcination temperatures also rendered coarse-grained powders. However, it was also found that the pH value employed in preparing gel powders affected the size of the calcined powders and that powders obtained using a slightly higher oxygen fugacity would have different particle sizes. A brief examination on the particle size variations revealed that a tendency for particle size increase existed if the pH increased from 3 to 7 (Table 3). This was attributed to the fact that higher pH would result in lower degrees of mixing for the Ni- and Fe-containing gels. Eventually, the higher pH environments would generate coarser gel particles, which subsequently required a higher temperature for nickel ferrite formation (Figs. 5 and 7). Meanwhile, starting materials with coarser particle sizes brought about coarser nickel ferrite powders.

The comparison between the two types of powders treated with and without additional air when calcined at 600°C revealed that the latter had particle sizes a hundred times larger than the former, a difference between 3000–5000 and 50–70 nm. The influence of pH on the particle size also prevailed. Those samples were calcined without additional air, since the DTA/TG examination (Fig. 3) disclosed a continuous weight gain, which occurred after the formation of Ni-ferrite. Moreover, the samples were thermally decomposed during annealing at higher temperatures (Figs. 4 and 5). The comparison between the two powders proves that the former (with air) has lower defects. Thus, it is clear that gels aged at lower pH solutions may be better mixed

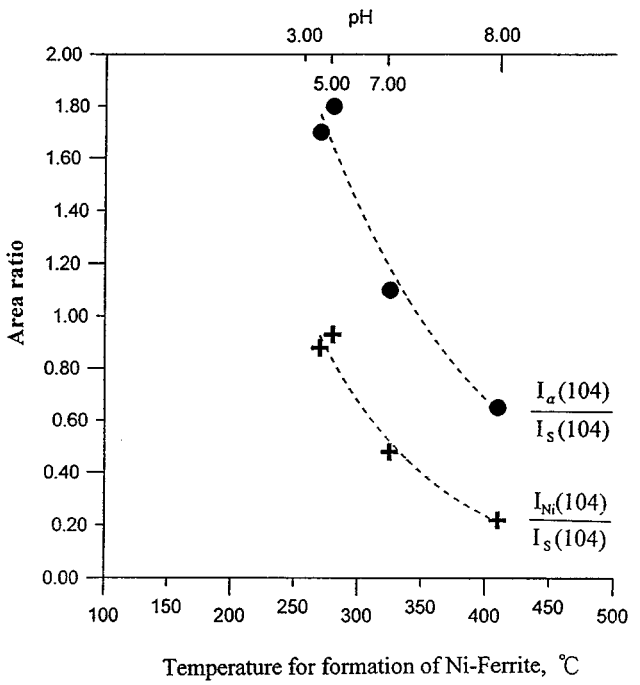

FIG. 5. Ni-ferrites with higher formation temperatures show higher stability when heated at 600°C/2 h. I_α, I_{Ni}, and I_S are XRD peak areas for a-Fe_2O_3, Ni metal, and Ni-ferrites, respectively.

and can be calcined to form nickel ferrite at lower temperatures. However, a proper oxygen fugacity must be provided or the nickel ferrite formed will have a higher rate of structural defects and will inevitably be decomposed into α-Fe_2O_3 and Ni metal at high temperatures. The decomposed powder, due to the presence of coarse-grained α-Fe_2O_3 and Ni metal particles (Fig. 7), gave a larger surface diameter which was a hundred times larger than the nickel

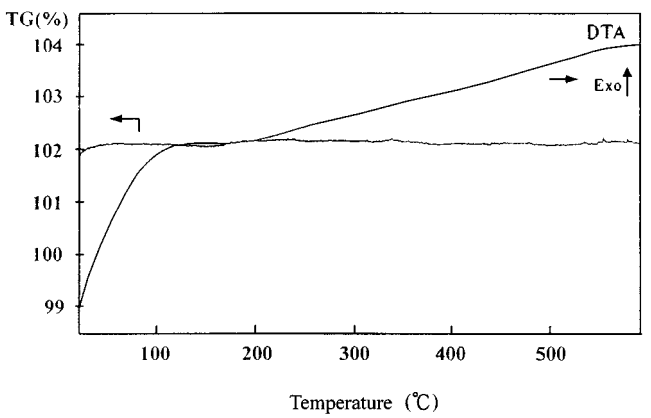

FIG. 6. DTA/TG curves for the Ni-ferrite powder obtained at 350°C/2 h with an air leak into the reaction system show no sign of weight gain.

TABLE 3
Particle Size (nm)[a] Variations of Ni–Ferrite Powders Obtained Using Starting Materials Treated with Different pH Values

Calc. temp. °C/2 h	pH 3	pH 5	pH 7	pH 8
350	8.53 ± 1	9.95 ± 1	10.7 ± 1	13.6 ± 1
450	15.5 ± 5	21.2 ± 5	23.3 ± 5	36.8 ± 5
600	3100 ± 500	4300 ± 500	5570 ± 500	2230 ± 500
350 (air)	10.9 ± 1	10.9 ± 1	11.8 ± 1	8.04 ± 1
600 (air)	48.9 ± 15	54.9 ± 15	66.0 ± 15	56.8 ± 15

[a] BET, surface area diameter.

ferrite particles. The proper addition of oxygen fugacity by opening the furnace door can suppress the defect development in the nickel ferrite crystallites and eventually prevent the thermal decomposition of the powders at higher temperature environments.

Nickel ferrite prepared using gel powders which were not well mixed for Ni and Fe ingredients as the starting materials requires a higher temperature for formation. The powder thus formed is coarse grained and lower in structural defects.

Detailed examinations for the sample that was aged at pH 8 confirm the conclusion (Table 3, pH 8). Since the 350°C/2 h calcination for the gel did not produce a nickel ferrite phase, the surface diameter of 8 nm, which was smaller than 11 nm, was the particle size of the starting materials. An increase in temperature for calcination to 450°C/2 h did result in the appearance of a nickel ferrite phase and a surface diameter of 13.6 nm was reached. As expected, this size was larger than 8–11 nm, because the nickel ferrite was formed via raw materials with particle sizes >8 nm and the formation temperature was >400°C. High temperature formed nickel ferrite powders will have fewer defects; thus, the thermal decomposition at 600°C for the sample yielded lower formation of α-Fe_2O_3 and Ni metal and a larger surface diameter of 2230 nm for the calcined powder obtained.

CONCLUSIONS

Ultrafine nickel ferrite powders can be prepared by the calcination of coprecipitated gel powders of Ni- and Fe-containing tartrates. The gel powder was a mixture of Ni and Fe tartrates. During thermal treatments, the mixture exhibited characteristics of the individual salt. Mixing homogeneity of the two salts strongly influenced the history of thermal reaction and the characteristics of the powder thus obtained. The nickel ferrite phase can be formed at the temperature range of 250 to 400°C. The prepared nickel

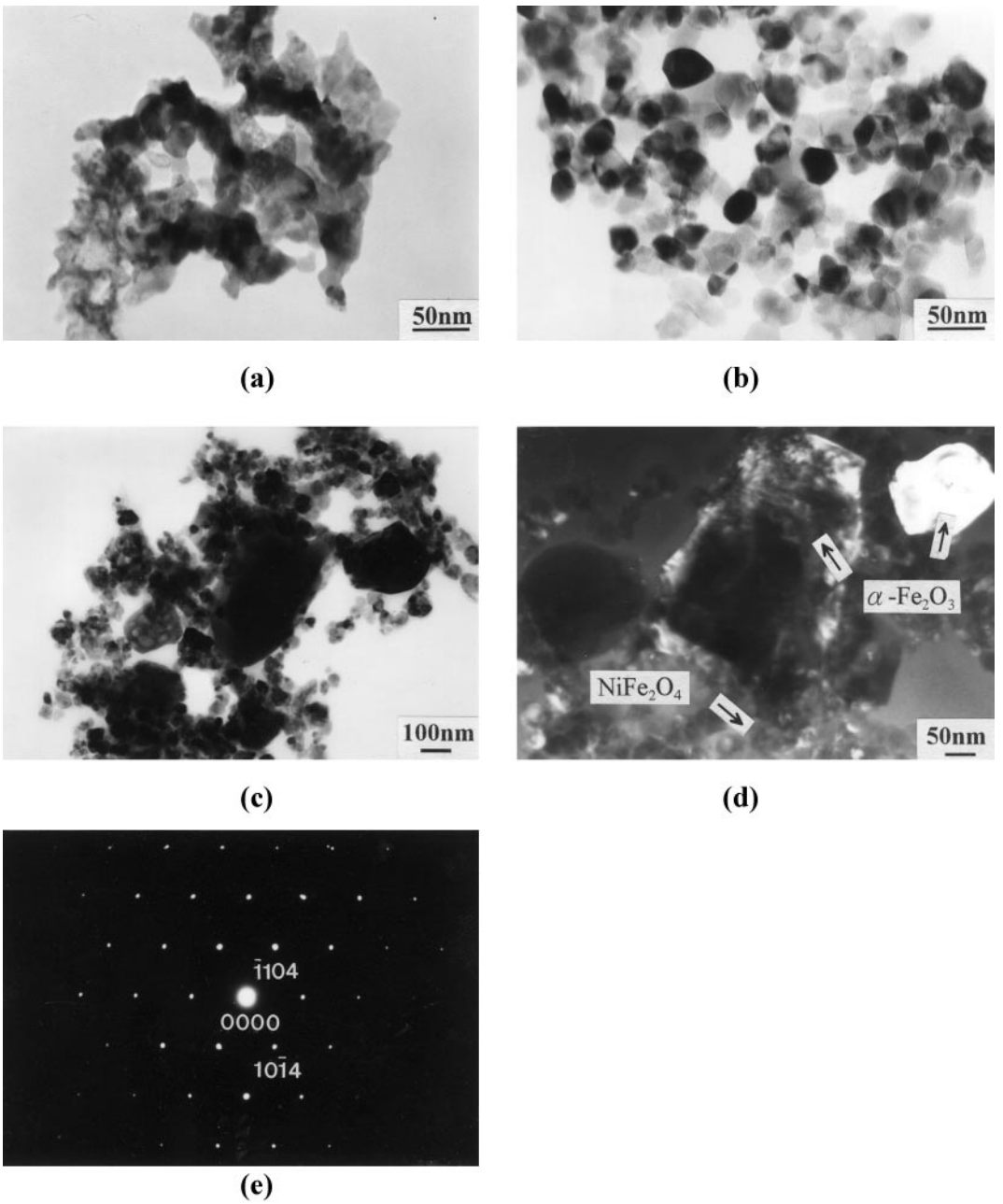

FIG. 7. TEM micrographs of nickel ferrite powders: (a) pH 5 powders calcined at 350°C for 2 h, (b) pH 5 powders calcined at 600°C for 2 h with an air leak into the calcination furnace, (c) pH 5 powders calcined at 600°C for 2 h obtained without an air leak into the calcination furnace, (d) the dark-field images of α-Fe_2O_3 particles, and (e) selected-area electron diffraction pattern of α-Fe_2O_3 phase.

ferrite powder showed a particle size of about 10 nm. Both the formation temperature and the formed particle size increased with the retrograde of the mixing state, possibly because of the increase in crystallite sizes of the intermediates (γ-Fe_2O_3 and NiO or Ni metal phases) by which the nickel ferrite powder was derived.

The defect nickel ferrite spinel was formed if the oxygen fugacity was not provided. The nickel ferrite powders thus formed, especially those obtained at lower calcination temperatures, were highly susceptible to thermal decomposition at higher temperatures. The decomposed powder, due to the presence of coarse-grained α-Fe_2O_3 and Ni metal particles, gave a surface diameter which is a hundred times larger than the nickel ferrite particles. A proper opening of the furnace door can suppress the defect development in the nickel ferrite crystallites and eventually prevent the thermal decomposition of the powders at higher temperature environments.

ACKNOWLEDGMENTS

We thank Dr. Y. H. Chang for his helpful discussions. This work was sponsored by the National Science Council of the Republic of China under Grant NSC 85-2216-E006-039.

REFERENCES

1. G. Economos, *J. Am. Ceram. Soc.* **42,** 628 (1959).
2. S. L. Blum and P. C. Li, *J. Am. Ceram. Soc.* **44,** 611 (1961).
3. J. Shimoiizaka and K. Nakatska, *Hyomen* **13,** 103 (1975).
4. S. Komarneni, E. Fregeau, E. Breval, and R. Roy, *J. Am. Ceram. Soc.* **71,** C-26 (1988).
5. A. H. Morrish and K. Haneda, *J. Appl. Phys.* **52,** 2496 (1981).
6. D. W. Johnson, Jr., *Am. Ceram. Soc. Bull.* **60,** 221 (1981).
7. C. H. Marcilly, P. Courty, and B. Belmon, *J. Am. Ceram. Soc.* **53,** 56 (1970).
8. H. Tamura and E. Matijevic, *J. Colloid Interface Sci.* **90,** 100 (1982).
9. P. Courty, H. Ajot, C. Marcilly, and B. Delmon, *Powder Tech.* **7,** 21 (1973).
10. J. J. Ritter and P. Maruthamuthu, *J. Mater. Syn. Proc.* **3,** 331 (1995).
11. A. Clearfield, A. M. Gadalla, W. H. Marlow, and T. W. Livingston, *J. Am. Ceram. Soc.* **72,** 1789 (1989).
12. T. Tsumura, A. Shimizu, and M. Inagaki, *J. Mater. Chem.* **3,** 995 (1993).
13. E. Matijevic, *Annu. Rev. Mater. Sci.* **15,** 483 (1985).
14. E. Matijevic, *Langmuir* **10,** 8 (1994).
15. C. L. Huang and E. Matijevic, *Solid State Ionics* **84,** 249 (1996).
16. E. Matijevic, *J. Europ. Ceram. Soc.* **18,** 1357 (1998).
17. M. Andrés-Vergés, C. de Julián, J. M. González, and C. J. Serna, *J. Mater. Sci.* **28,** 2962 (1993).
18. K. Vidyasagar, J. Gopalakrishnan, and C. N. R. Rao, *Inorg. Chem.* **23,** 1206 (1984).
19. P. Karen and A. Kjekshus, *J. Am. Ceram. Soc.* **77,** 547 (1994).
20. K. Okada, and N. Ôtsuka, *J. Am. Ceram. Soc.* **69,** 652 (1986).
21. S. Komarneni, R. Roy, E. Breval, M. Ollinen, and Y. Suwa, *Adv. Ceram. Mater.* **1,** 87 (1986).
22. N. G. Eror, Jr. and T. M. Loehr, *J. Solid State Chem.* **12,** 319 (1975).
23. A. M. Gadalla, *Thermochi. Acta.* **164,** 21 (1990).
24. C. Barriga, V. Barron, R. Gancedo, M. Gracia, J. Morales, J. L. Tirado, and J. Torrent, *J. Solid State Chem.* **77,** 132 (1988).